Design of Highly Selective Metamaterials for Sensing Platforms

Kyungjun Song and Pinaki Mazumder, *Fellow, IEEE*

***Abstract*— This paper presents a methodology to construct novel label-free sensing platforms using carefully engineered materials (metamaterials) that have dimensions considerably smaller than the operating wavelength, λ. This paper demonstrates that highly selective sensing platforms can be achieved by using metamaterials consisting of periodic arrays of capacitive and inductive elements. Specifically, this paper gives the design of the following four basic sensing parameters of sensing platforms: 1) resonant frequency ω_0; 2) resonant frequency shift $\Delta\omega_0$; 3) bandwidth B; and 4) transmission ratio T. Using this approach, the bandwidth B and resonant frequency ω_0 can easily be modulated by using different combination sets of metallic patch elements and metallic wire elements. Equivalent circuit analysis and numerical methods have been applied to determine the basic sensing design rules for constructing periodic arrays of capacitive and inductive elements, and the efficiency of the obtained label-free sensing architectures has been evaluated. The overall contribution of this paper is to develop a methodology for designing highly selective biosensors by optimizing the dimensions of underlying circuit at the subwavelength scale.**

***Index Terms*— Biosensors, frequency selective surfaces, label-free sensing, metamaterial, plasmonics, selectivity, sensitivity.**

I. Introduction

ARTIFICIALLY engineered metamaterials warrant innovative research to develop novel design methodologies by exploiting exotic electromagnetic (EM) physical behaviors that are not normally found to occur in nature [1], [2]. For instance, specific resonant elements can be used to generate extraordinary EM behaviors, thereby enabling the design of novel devices for enhancing resonant behaviors. Most metamaterials are based on split-ring resonators (SRRs) or similar geometries in order to achieve extraordinary physical behaviors for promising applications such as the fabrication of negative refractive materials [3], superlenses [4], smart power management applications [5], acoustic devices [6], and cloaking devices [7], [8].

Manuscript received January 15, 2013; revised March 12, 2013; accepted April 16, 2013. Date of publication April 30, 2013; date of current version August 6, 2013. This work was supported in part by the Army Research Office under Grant W911NF-10-1-0229 and the Korea Institute of Machinery and Materials under Grant NK175B. The associate editor coordinating the review of this paper and approving it for publication was Dr. Shoushun Chen.

K. Song is with the Department of Nature-Inspired Nano-convergence System, Korea Institute of Machinery and Materials, Daejoen 305-343, Korea (e-mail: songk@kimm.re.kr).

P. Mazumder is with the Department of Electrical and Computer Science Engineering, University of Michigan, Ann Arbor, MI 48109 USA (e-mail: mazum@eecs.umich.edu).

Color versions of one or more of the figures in this paper are available online at http://ieeexplore.ieee.org.

Digital Object Identifier 10.1109/JSEN.2013.2260143

More recently, increasing interest has been evinced in developing sensing platforms based on SRR arrays [9], [10]. For example, Hu Tao et al. have successfully developed label-free sensing platforms with SRR elements patterned on paper [11]. The EM resonant behaviors produced from SRR elements provide unique EM signatures in sensor applications. Because the resonant frequency ω_0 can be easily modulated by the device structure rather than composition, sensing parameters such as the resonant frequency ω_0 and bandwidth B can be easily controlled and achieved by properly designed subwavelength elements. Nonetheless, when compared with the performance of conventional plasmonics devices, SRR-metamaterial biosensors require further improvements in their sensing capability particularly in the light of their current low EM localization and low selectivity generated from the basic physics of metamaterials.

In this study, we introduce novel approaches for the design of label-free sensing platforms with miniaturized subwavelength elements. These architectures are based on parallel combinations of periodic arrays of metallic patch elements and metallic wire elements. In particular, this building block creates a highly compact resonator, in which the wavelength of the resonant frequency is considerably larger than the periodicity of the patterned elements. Recently, investigations of simple frequency selective surfaces (FSSs) have been carried out both numerically and experimentally [12]–[15]. Even though our label-free sensors operate in the microwave spectrum, the basic design methodologies can be easily applied to terahertz or infrared frequencies by scaling down the device size.

Our study demonstrates the working of miniaturized sensing platforms with a highly selective spectrum. In particular, we investigate four basic sensing parameters including the resonant frequency ω_0, resonant frequency shift $\Delta\omega_0$, bandwidth B, and transmission ratio T. The basic design rules of metamaterial sensors based on parallel LC elements indicate that large values of capacitance C and inductance L are essential for the miniaturization of sensing devices because of the large wavelength λ. In addition, large values of C and small values of L are required to achieve sensing operation in a narrowband spectrum when fundamental parallel LC resonators are used. However, small C values are useful for obtaining a large $\Delta\omega_0$ for a given refractive index modulation δn. Therefore, it is essential to optimize the capacitance C and the inductance L to obtain the desired sensing platforms. For example, in order to increase sensitivity, we design a periodic array size of patch elements larger than the periodic array of size of wire elements. On the other hand, in order

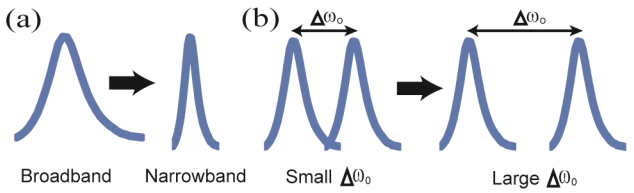

Fig. 1. The label-free sensing capability depends on narrowband spectrum B and a large resonant shift $\Delta\omega_0$ for a given δn value.

to enhance selectivity, we design a periodic array of size of patch elements smaller than the periodic array of size of wire elements. In addition, for a highly selective resolution, we use loop elements and complimentary loop elements instead of wire elements and patch elements.

II. Limitations of Label-Free Sensors Based on Split-Ring Resonator Arrays

The detection of DNA and other molecules by sensing platforms can be identified by the shift in the resonant frequency $\Delta\omega_0$ due to the alteration of capacitance by the added chemical molecules. Ideal label-free sensors provide large $\Delta\omega_0$ values for a given δn value and a narrowband spectrum B, as illustrated in Fig. 1. Thus, label-free sensing ability based on metamaterials can be explained by four fundamental physical factors: (1) Resonant frequency ω_0 related to the miniaturization of sensing architectures, (2) resonant frequency shift $\Delta\omega_0$ at δn related to highly localized electric fields, (3) narrowband spectrum with high Q factor, and (4) transmission $T = P_T / P_I$ related to the sensing device performance. In order to obtain a sharp resonant spectrum with a strong localized EM confinement, it is essential to optimize the metamaterial sensor architectures. In this study, we obtain the abovementioned four basic design parameters using two fundamental methods: equivalent circuit analysis and numerical simulation (such as finite element simulation). An equivalent circuit analysis provides an intuitive physical understanding of the design parameters, and the finite element method (FEM) enables the detailed calculation of circuit parameters such as resonant frequency ω_0, resonant frequency shift $\Delta\omega_0$, bandwidth B, and transmission T.

Most current metamaterial sensing architectures are based on SRRs, thereby enabling miniaturization of device elements at a subwavelength scale. The basic physics of SRRs can be determined by the equivalent capacitance C and inductance L, where the capacitance C is determined by the gap length of the SRR and the dielectric material used, and the inductance L is calculated by the path current of SRRs. In order to determine the basic design rules of sensing architectures based on SRRs, we use equivalent circuit analysis because SRR resonators can simply be represented by the series combination of capacitor C and inductor L, as illustrated in Fig. 2(a) [16]–[18]. The transmission T can be simply expressed by

$$T = \left| \frac{2Z}{2Z + Z_0} \right|^2 = \left| \frac{2}{2 + Z_0 \left(\frac{j\omega C}{1-\omega^2 LC} \right)} \right|^2 \quad (1)$$

with $Z = 1/j\omega C + j\omega L$. Thus, the resonant frequency ω_0, quality factor Q, bandwidth B, and transmission T can be

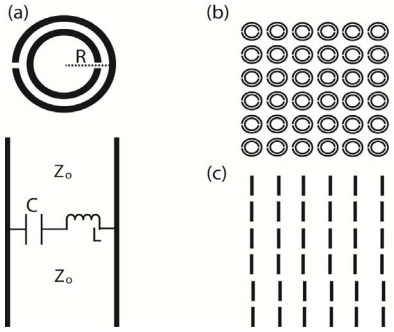

Fig. 2. (a) Split-ring resonator (SRR) arrays can be simply regarded as series arrays with capacitance C and inductance L. In this representation, the conducting loss produced from metallic conductors is ignored. (b) Sensing architectures consisting of a periodic array of SRR elements. (c) Sensing architectures consisting of a periodic array of metallic wire elements.

calculated as

$$\omega_0 \sim \sqrt{\frac{1}{LC}},\ Q \sim \frac{Z_0}{2}\sqrt{\frac{L}{C}}B \sim \frac{2}{Z_0}\sqrt{\frac{C}{L}},\ \text{and}\ T \sim 0\ (\text{at}\ \ \omega = \omega_0) \quad (2)$$

High selectivity with a narrow spectral bandwidth can be achieved by large L/C values. However, the inductance L and capacitance C of SRR elements are proportional to the radius R of the ring elements, thereby limiting the achievement of a very narrow spectral bandwidth; such SRR circuit elements are shown in Fig. 2(b). As illustrated in Fig. 2(c), instead of using an SRR array, we can use different periodic structures with large L/C values, thereby achieving the required narrowband spectrum. However, these architectures are highly limited in terms of the miniaturization of elements because small ω_0 result for a given δn value due to negligible EM resonant coupling.

III. Basic Sensing Architectures Based on Metamaterials

In this study, we focus on the use of metamaterial architectures to demonstrate highly miniaturized sensor architectures. The basic sensing designs are based on parallel LC resonators consisting of periodic arrays of capacitive and inductive elements as shown in Fig. 3(a). The metallic patch elements can be considered as capacitive elements behaving like low-pass filters. The metallic wire elements can be regarded as inductive elements acting like high-pass filters. In contrast to SRR structures, there are more design variables available to tailor bandwidth B and resonant frequency ω_0 because we can easily design the L and C values independently. The basic topology of the unit cell of the basic sensors is determined by the periodic size of the capacitive elements (D_1), the periodic size of the inductive elements (D_2), the gap between patch elements (g), the width of wire elements (w), thickness of patch elements (t_1), thickness of wire elements (t_2), and thickness of the substrate (t) as illustrated in Fig. 3(b).

In order to verify the basic sensing mechanism based on the capacitance variation in the metallic patches upon attaching biomolecules and chemical molecules, we consider the molecular binding event within the subwavelength gaps of patch elements, as shown in Fig. 3(c). In particular, Fig. 4 shows the

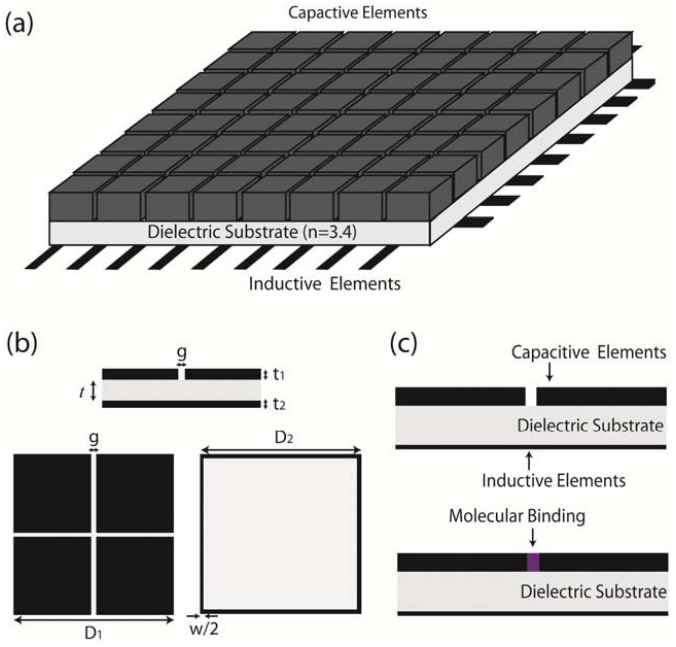

Fig. 3. (a) Sensing platforms consisting of periodic arrays of capacitive and inductive elements. (b) The basic topology of a unit cell can be described by the periodic distance D_1 of a patch element, the periodic distance D_2 of a wire element, gap g between a patch element, width w of a wire element, thickness t_1 of a patch element, thickness t_2 of a wire element, and thickness t of the substrate. (c) Side view of unit cell without and with molecular binding.

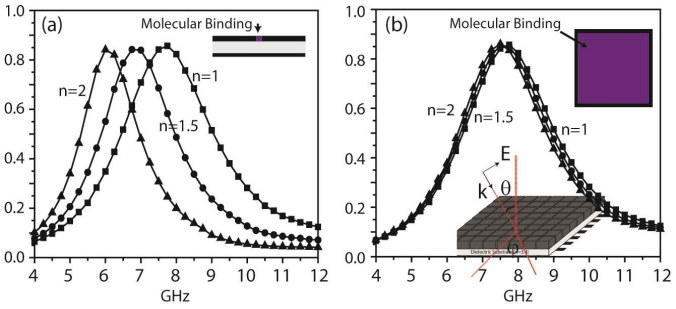

Fig. 4. Transmission ratios of sensing architecture obtained for different values of refractive index n. (a) Transmission ratios obtained at various refractive indices n within subwavelength capacitive elements. (b) Transmission coefficients obtained at various refractive indices n within subwavelength inductive elements.

transmission $T = P_T/P_I$ induced by different refractive indices n within the subwavelength metallic gap g. The transmission coefficients can be obtained by using an FEM based on linked boundary conditions [19]. The normal incident TM wave ($\theta = 0$, $\varphi = 0$), shown in the inset of Fig. 4(b), is used to calculate the transmission coefficients of the sensor devices with the following design parameters: $D_1 = 5$ mm, $D_2 = 5$ mm, $t = 0.5$ mm, $t_1 = 0.2$ mm, $t_2 = 0.2$ mm, $g = 0.2$ mm, and dielectric substrate with $n = 3.4$ (as illustrated in Fig. 3(b)). The transmission T of the sensing architectures can be calculated as the ratio of the transmitted and incident power. As shown in Fig. 4(a), the required value of $\Delta\omega_0$ can easily be achieved by using different refractive indices n. However, the transmission behavior due to the inductance L induced by different surrounding substrates is almost negligible, as observed in Fig. 4(b). Therefore, we only consider the metamaterial sensing architectures by modulating the capacitance C within the subwavelength metallic gap between patch elements.

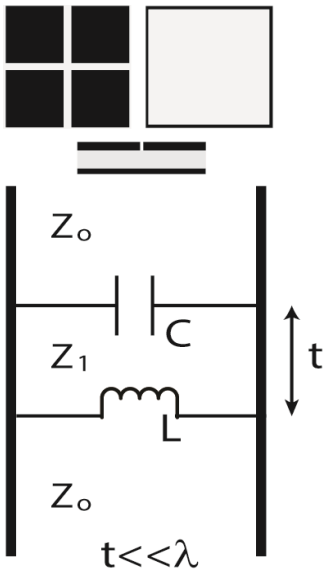

Fig. 5. Equivalent circuit model of parallel LC resonators as illustrated in Fig. 3(a). The parameter $t$represents the thickness of the substrate. The parameter Z_0 denotes the wave impedance in air, and $Z_1 = Z_0/n$ indicates the wave impedance in the dielectric material.

IV. Bandwidth Design by Different Combinations of Periodic Elements

In order to explain the sensing parameters based on metamaterials, we use the equivalent circuit analysis illustrated in Fig. 5. The equivalent circuit model can be expressed as a parallel LC circuit whose values are determined by a short transmission line t and wave impedance $Z_1 = Z_0/\sqrt{\varepsilon}$. The ABCD matrix for this case can be written as:

$$\begin{bmatrix} A & B \\ C & D \end{bmatrix} = \begin{bmatrix} 1 & 0 \\ \frac{1}{Z_U} & 1 \end{bmatrix} \begin{bmatrix} \cos\beta t & jZ_1 \sin\beta t \\ \frac{j\sin\beta t}{Z_1} & \cos\beta t \end{bmatrix} \begin{bmatrix} 1 & 0 \\ \frac{1}{Z_L} & 1 \end{bmatrix} \quad (3)$$

with $Z_U = 1/j\omega C$ for the metallic patch elements and $Z_L = j\omega L$ for the metallic wire elements. For a very small thickness value $t \ll \lambda$, $\beta t \sim 0$, and thus, the ABCD matrix can be expressed as:

$$\begin{bmatrix} A & B \\ C & D \end{bmatrix} \sim \begin{bmatrix} 1 & 0 \\ \frac{1}{Z_U} & 1 \end{bmatrix} \begin{bmatrix} 1 & jZ_1\beta t \\ \frac{j\beta t}{Z_1} & 1 \end{bmatrix} \begin{bmatrix} 1 & 0 \\ \frac{1}{Z_L} & 1 \end{bmatrix} \quad (4)$$

Consequently, the transmission T can be calculated as:

$$T = \left| \frac{2}{2 + Z_1\beta t\left(\frac{1}{\omega L} - \omega C\right) + jZ_0\left(\frac{1}{\omega L} - \omega C\right) + jZ_0\left(\frac{\beta t}{Z_1} + \frac{C}{L}\frac{Z_1\beta t}{1} + \frac{Z_1\beta t}{Z_0^2}\right)} \right|^2 \quad (5)$$

From this equation, the resonant frequency ω_0 can be expressed as:

$$\omega_0 \sim \frac{1}{\sqrt{CL}} \quad (6)$$

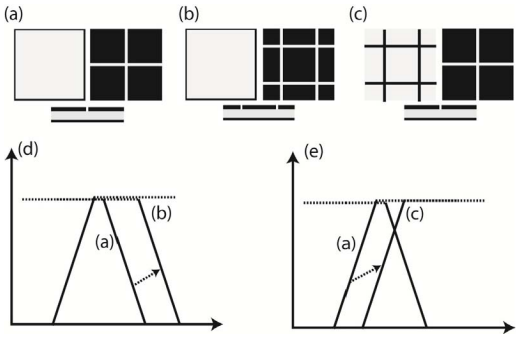

Fig. 6. (a) Parallel combination of inductive and capacitive elements, both having same period. (b) Parallel combination of inductive and capacitive elements with a small C/L. (c) Parallel combination of inductive elements and period of inductive elements with a large C/L. (d) A broadband spectrum can be achieved using a small period for capacitive elements and a large period for inductive elements. (e) A narrowband spectrum can be obtained using a small period for inductive elements and large period for inductive elements.

Consequently, the quality factor Q and bandwidth B can be written as:

$$Q \sim \frac{Z_0}{2}\sqrt{\frac{C}{L}} \quad \text{and} \quad B \sim \frac{2}{Z_0}\sqrt{\frac{L}{C}} \tag{7}$$

As mentioned in previous section, a high quality factor Q can be obtained in SRR arrays with large values of L/C because of the presence of series LC resonators. However, from Eqn. (7), we observe that a high quality factor Q of parallel LC circuits based on wire and patch elements can be achieved by a large C/L. The transmission T at $\omega = \omega_0$ can be also approximately calculated as:

$$T = \left| \frac{2}{2 + jZ_0\frac{\beta t}{Z_1}\left(1 + \frac{CZ_1^2}{L} + \frac{Z_1^2}{Z_0^2}\right)} \right|^2 \tag{8}$$

In addition, Eqn. (8) indicates that low transmission can be achieved using a large C/L and high transmission can be obtained using a small C/L.

The approximate L values of the metallic wire elements and C values of the metallic patch elements are given as [12]:

$$C = \varepsilon\varepsilon_0\frac{2D_1}{\pi}\log\left(\frac{1}{\sin\frac{\pi g}{2D_1}}\right) \quad \text{and} \quad L = \mu_0\frac{2D_2}{\pi}\log\left(\frac{1}{\sin\frac{\pi w}{2D_2}}\right) \tag{9}$$

As observed from Eqn. (9), the capacitance C and inductance L are almost proportional to the periodic size of the patch elements D_1 and the periodic size of the wire elements D_2, respectively. Thus, we can easily modulate sensing parameters such as the resonant frequency ω_0, bandwidth B, and transmission T by using different design sets of periodicities for the subwavelength capacitive and inductive elements. For example, bandwidth B and transmission T can be easily modulated by designing various combination sets of periodic arrays of metallic wires and metallic patches as shown, in Figs. 6(a)–(c).

Next, the variation in bandwidth B and transmission T can be understood via graphical analysis, as illustrated in Figs. 6(d) and (e). The normal bandwidth can be achieved by structures consisting of a periodic array of patch and wire elements, both having the same period. In order to increase bandwidth, we design a periodic array size of patch elements smaller than the periodic array size of the wire elements. Consequently, the cutoff frequency of the low-pass filter moves to the high frequency region, thereby achieving the required broadband spectrum along with a high transmission ratio, as shown in Fig. 6(d). On the other hand, in order to decrease bandwidth, we can reduce the array size of the metallic wire elements when compared with that of the periodic array of the patch elements. In this case, the cutoff frequency of the high-pass filter moves to the high frequency region, thereby leading to a narrow spectral response and low transmission ratio, as shown in Fig. 6(e). However, both cases provide a short wavelength λ in a given unit cell when compared with the normal FSS architecture, thus limiting the scale of miniaturization.

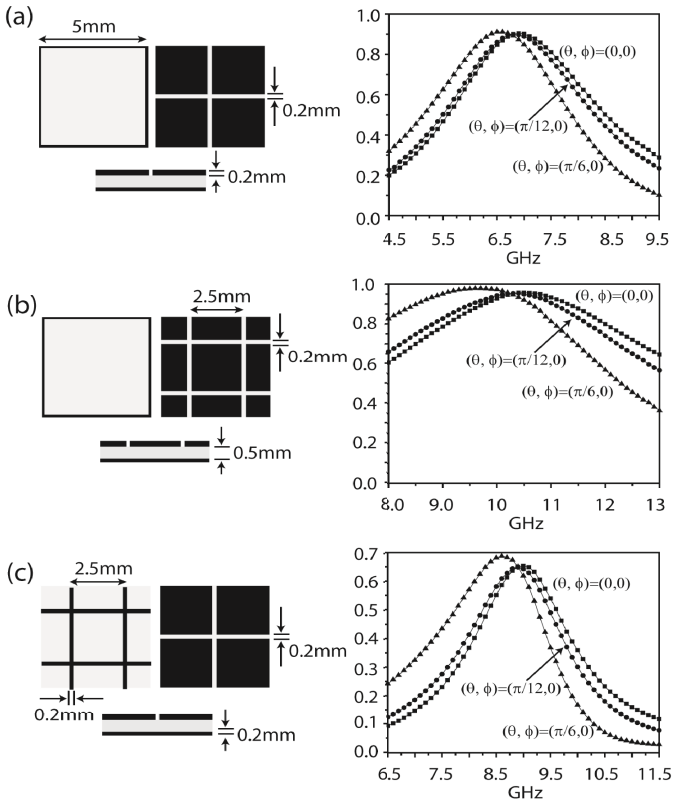

Fig. 7. Transmission ratios of sensing architectures obtained using incident frequency with different angles $\theta = 0$, $\pi/12$, and $\pi/6$, respectively. (a) Sensor device design parameters: $D_1 = 5$ mm, $D_2 = 5$ mm, $t = 0.5$ mm, $t_1 = 0.2$ mm, $t_2 = 0.2$ mm, $g = 0.2$ mm, and refractive index of dielectric substrate $n = 3.4$. (b) Sensor device design parameters: $D_1 = 2.5$ mm, $D_2 = 5$ mm, $t = 0.5$ mm, $t_1 = 0.2$ mm, $t_2 = 0.2$ mm, $g = 0.2$ mm, and refractive index of dielectric substrate $n = 3.4$. (c) Sensor device design parameters: $D_1 = 5$ mm, $D_2 = 2.5$ mm, $t = 0.5$ mm, $t_1 = 0.2$ mm, $t_2 = 0.2$ mm, $g = 0.2$ mm, and refractive index of dielectric substrate $n = 3.4$.

In order to verify the control of bandwidth and transmission using different combination sets of capacitive and inductive elements, the transmission coefficients of three combination sets of capacitive and inductive elements are calculated and compared, as shown in Fig. 7. In order to examine the effect

TABLE I
PHYISICAL SENSING PARAMETERS FOR DEVICES SHOWN IN FIG. 7

	Resonant Frequency (ω_0)	Unit cell at ω	Bandwidth ($\omega_H - \omega_L/\omega_0$)	Transmission Ratio (P_T/P_I)
Type I	6.9 GHz	D $\sim 0.110\lambda$	Normal 0.463	0.9
Type II	10.4 GHz	D $\sim 0.175\lambda$	Broadband 0.579	0.90
Type III	8.9 GHz	D $\sim 0.150\lambda$	Narrowband 0.247	0.65

of incident angle θ, we calculate the transmission coefficients for value of $\theta = 0$, $\pi/12$, and $\pi/6$, respectively. It is observed that the transmission responses T and resonant frequency ω_0 are not strongly dependent on the angle of incident frequency. The basic physical sensing parameters for the three types of architectures are summarized in Table I. The 3-dB bandwidth, which is considered as the frequency regime within the spectral range, is above half its maximum value. To estimate the bandwidth, we use the simple equation $B = (\omega_H - \omega_L)/\omega_0$ where ω_H denotes the high band edge and ω_L indicates the low band edge. As illustrated in Fig. 7(a), the sensing architectures with capacitive and inductive elements, both having the same period, correspond to a normal bandwidth with a resonant frequency $\omega_0 \sim 6.9$ GHz, thereby corresponding to D $\sim 0.110\lambda$, bandwidth B ~ 0.463, and transmission ratio T ~ 0.9. However, sensing architectures with a large L/C show a broadband spectrum B ~ 0.579, thereby corresponding to D $\sim 0.175\lambda$ and transmission T ~ 0.9, as shown in Fig. 7(b). Finally, sensing architectures with a small L/C show a narrowband spectrum B ~ 0.2471 with resonant frequency $\omega_0 \sim 8.9$ GHz and transmission $T \sim 0.65$.

V. SENSITIVITY DESIGN BASED ON PATCH ELEMENTS AND WIRE ELMENTS

In this section, in order to examine the sensitivity of sensing architectures, we investigate the variation in $\Delta\omega_0$ by modulating the capacitance C of the capacitive elements induced by different chemical concentrations present on the metallic patch elements. The resonant frequency ω_0 can be expressed as $\omega_0 \sim \sqrt{1/LC}$. To estimate the change in the resonance frequency $\Delta\omega_0$ based on $C + \Delta C$, ω_0 can be expressed as $\omega_0 \sim \sqrt{1/L\,(C + \Delta C)}$. The variation ΔC can be obtained by modulating the refractive index δn within the subwavelength gap between a periodic array of patch elements. The ration $\Delta\omega_0/\omega_0$ can be expressed as:

$$\frac{\Delta\omega_0}{\omega_0} = \left[1 - \frac{1}{\sqrt{1 + \frac{\Delta C}{C}}}\right] \tag{10}$$

It is essential to increase the ratio ΔC/C in order to enhance the value of $\Delta\omega_0/\omega_0$. First, we can decrease the subwavelength gap g between the patch elements to increase ΔC because ΔC is inversely proportional to the subwavelength gap between the patch elements. The transmitted ratios of metamaterials with subwavelength gaps of $g = 0.4$ mm and $g = 0.2$ mm are calculated and shown in Figs. 8(a) and (b). The architecture with a small gap of $g = 0.2$ mm between the patch elements provides a low resonant frequency and narrow bandwidth when compared with those for the architecture with a wide gap of $g = 0.4$ mm between the patch elements.

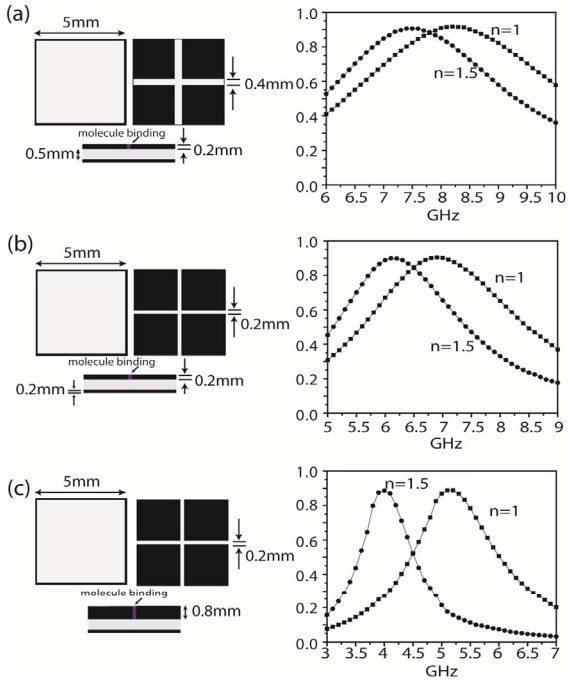

Fig. 8. Transmission ratios for three different sensing architectures obtained using normal incident frequency without and with molecular binding (n = 1.5). (a) Sensor device design parameters: $D_1 = 5$ mm, $D_2 = 5$ mm, t = 0.5 mm, $t_1 = 0.2$ mm, $t_2 = 0.2$ mm, g = 0.4 mm, and refractive index of substrate $n = 3.4$. (b) Sensor device design parameters: $D_1 = 5$ mm, $D_2 = 5$ mm, t = 0.5 mm, $t_1 = 0.2$ mm, $t_2 = 0.2$ mm, g = 0.2 mm, and refractive index of substrate $n = 3.4$. (c) Sensor device design parameters: $D_1 = 5$ mm, $D_2 = 5$ mm, t = 0.5 mm, $t_1 = 0.8$ mm, $t_2 = 0.2$ mm, g = 0.2 mm, and refractive index of substrate $n = 3.4$.

Second, we change the capacitance C by increasing the thickness of the capacitive elements. This approach enables increase in C and ΔC. Fig. 8(c) shows the transmission coefficient of the sensing architecture with thickness $t_1 = 0.8$ mm. It is observed that the resonant frequency ω_0 at $n = 1$ is 5.25 GHz, thereby corresponding to miniaturized elements with a periodic distance D $\sim 0.088\lambda$. The required narrowband B and a large $\Delta\omega_0$ can also be achieved by using capacitive elements with large thickness ($t_1 = 0.8$ mm).

On the other hand, in order to enhance the sensitivity of the sensing architectures, we can obtain a large value of $\Delta\omega_0$ for a given $\delta n/n$ by reducing the size of the capacitive elements in a given unit cell, as illustrated in Fig. 9. This is because the ratio ΔC/C can be enhanced by decreasing the capacitance C (Eqn. (9)). Fig. 9 shows the calculated transmission response of the sensing architectures with a periodic array of capacitive elements with $D_1 = 2.5$ mm and a periodic array of inductive elements with $D_2 = 5$ mm. This architecture provides a resonant frequency $\omega_0 \sim 7.7$ GHz at $n = 1$, thereby corresponding to miniaturized elements with a unit cell dimension of $D_2 \sim 0.128\lambda$ and $\Delta\omega_0 \sim 2$ GHz at $\delta n = 0.5$. Even though a large $\Delta\omega_0$ value at small δn can

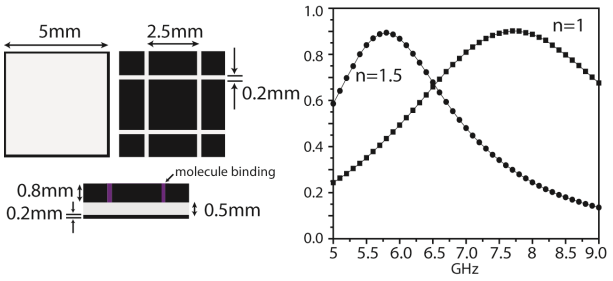

Fig. 9. Transmission ratios of sensing architecture at normal incident frequency without molecule binding (n = 1) and with molecule binding (n = 1.5). Sensor device design parameters: $D_1 = 2.5$ mm, $D_2 = 5$ mm, t = 0.5 mm, $t_1 = 0.8$ mm, $t_2 = 0.2$ mm, g = 0.2 mm, and refractive index of substrate $n = 3.4$.

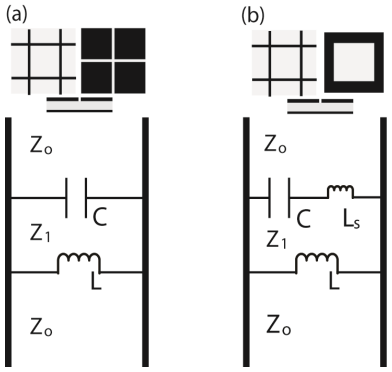

Fig. 10. (a) Equivalent circuit models of periodic arrays of patch and wire elements. (b) Equivalent circuit models of periodic arrays of loop and wire elements. Loop elements can be interpreted as series LC resonators.

be obtained by using small capacitive elements, the resulting broadband response is not desirable for miniaturized sensor applications.

VI. Selecivity Design Using Loop Elements and Wire Elments

Thus far, we have focused on the use of metallic patch elements to provide capacitive elements in the equivalent LC resonators. However, the required narrowband spectrum and the miniaturization of the elements of sensor devices can be achieved by using metallic loop elements instead of metallic patch elements [14], [15]. From the equivalent circuit analysis, it is noted that loop elements provide a capacitive element C and an additional inductive element L_s, thereby corresponding to an equivalent series *LC* resonator. Fig. 10 shows the basic equivalent circuit model of sensing architectures with wire elements and loop elements. To study transmission behavior due to inductance L_s generated by the loop elements, we use the ABCD transmission matrix. The ABCD transmission matrix can be written as:

$$\begin{bmatrix} A & B \\ C & D \end{bmatrix} \sim \begin{bmatrix} 1 & 0 \\ \frac{1}{Z_U} & 1 \end{bmatrix} \begin{bmatrix} 1 & jZ_1\beta t \\ jY_1\beta t & 1 \end{bmatrix} \begin{bmatrix} 1 & 0 \\ \frac{1}{Z_L} & 1 \end{bmatrix} \quad (11)$$

with $Z_U = 1/j\omega C + j\omega L_s$ (loop elements) and $Z_L = j\omega L$ (wire elements). From this equation, the resonant frequency ω_0 can be calculated as

$$\omega_0 \sim \frac{1}{\sqrt{C(L + L_s)}} \quad (12)$$

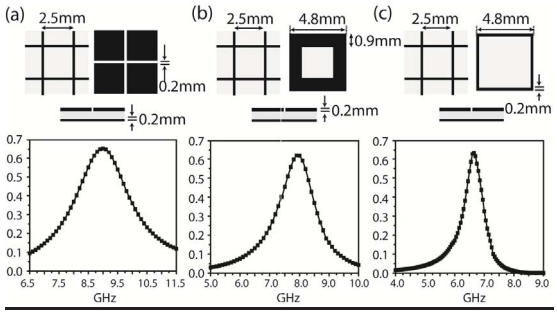

Fig. 11. Transmission ratios for three different sensing architectures obtained with angles of incident frequency $\theta = 0$, $\pi/12$, and $\pi/6$. (a) Patch and wire elements with design parameters $D_1 = 5$ mm, $D_2 = 2.5$ mm, t = 0.5 mm, $t_1 = 0.2$ mm, $t_2 = 0.2$ mm, g = 0.2 mm, and refractive index of substrate $n = 3.4$. (b) Loop and wire elements with design parameters $D_1 = 5$ mm, $D_2 = 2.5$ mm, t = 0.5 mm, $t_1 = 0.2$ mm, $t_2 = 0.2$ mm, g = 0.2 mm, and refractive index of substrate $n = 3.4$. The width of the loop is $w_2 = 0.9$ mm. (c) Loop and wire elements with design parameters $D_1 = 5$ mm, $D_2 = 2.5$ mm, t = 0.5 mm, $t_1 = 0.2$ mm, $t_2 = 0.2$ mm, g = 0.2 mm, and refractive index of substrate $n = 3.4$. The width of the loop element is $w_2 = 0.2$ mm.

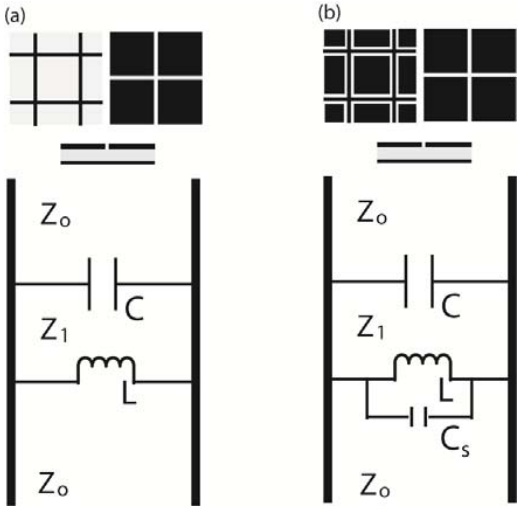

Fig. 12. (a) Equivalent circuit models of patch elements and wire elements. (b) Equivalent circuit models of patch elements and complementary loop elements. Complementary loop elements can be regarded as parallel LC resonators.

From Eqn. (12), a highly miniaturized architecture can be obtained by the inclusion of L_s. In addition, a narrow spectral response can be also achieved as

$$B \sim \frac{2L}{Z_0}\sqrt{\frac{1}{C(L + L_s)}} \quad (13)$$

In order to examine the sensing parameters influenced by L_s, we compare with transmission behavior of loop elements with different widths, as shown in Fig. 11. For instance, the sensing architecture based on loop elements with a large width of $w_2 = 0.9$ mm yields a resonant frequency $\omega_0 \sim 7.9$ GHz and bandwidth B $\sim$ 0.177. In order to increase sensing performance in terms of size and bandwidth, loop elements with a short width of $w_2 = 0.2$ mm can yield a low resonant frequency $\omega_0 \sim 6.6$ GHz and a narrow bandwidth $B \sim 0.125$.

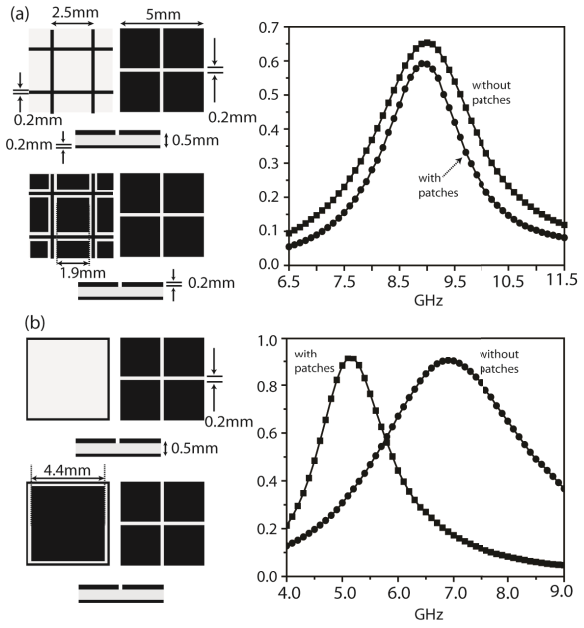

Fig. 13. Transmission ratios for different sensing architectures obtained with normal incident frequency. (a) Patch and wire elements with design parameters $D_1 = 5$ mm, $D_2 = 2.5$ mm, t = 0.5 mm, $t_1 = 0.2$ mm, $t_2 = 0.2$ mm, g = 0.2 mm, and refractive index of substrate $n = 3.4$. Design parameters of additional patch elements : A = 1.9 mm. (b) Patch and wire elements with design parameters $D_1 = 5$ mm, $D_2 = 5$ mm, t = 0.5 mm, $t_1 = 0.2$ mm, $t_2 = 0.2$ mm, g = 0.2 mm, and refractive index of substrate $n = 3.4$. Design parameters of additional patch elements : A = 4.4 mm.

VII. Selecivity Design Using Patch Elements Vand Complimentary Loop Elements

A narrow spectral bandwidth for the sensing architectures can be also achieved by the inclusion of patch elements within the metallic wires, as shown in Fig. 12. These architectures are termed complementary loop metamaterials. The complementary loop elements can be expressed in terms of the equivalent parallel *LC* resonators, as shown in Fig. 12(b). Thus, the impedance Z_L of the complementary loop elements can be written as:

$$Z_L = \frac{j\omega L}{1 - \omega^2 L C_s} \tag{14}$$

The resonant frequency ω_0 can be approximately calculated using the ABCD matrix as

$$\omega_0 \sim \sqrt{\frac{1}{L\,(C + C_s)}} \tag{15}$$

The bandwidth B is approximately given by

$$B \sim \frac{2}{Z_0}\sqrt{\frac{L}{C + C_s}} \tag{16}$$

Fig. 13 shows how the value of the additional capacitance C_s generated by the complementary loops influences the transmission behaviors of the sensing architectures. Thus, we consider different patch sizes with A = 1.9 mm and A = 4.4 mm within metallic wire elements as illustrated in Fig. 13. As a result, the complementary loop elements based on wire and patch elements for A = 1.9 mm provide a small

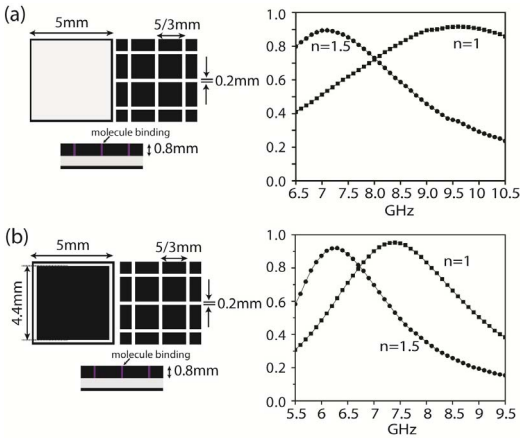

Fig. 14. Transmission ratios for three different sensing architectures obtained at normal incident frequency without and with molecule binding (n = 1.5). (a) Patch and wire elements with design parameters $D_1 = 5/3$ mm, $D_2 = 5$ mm, t = 0.5 mm, $t_1 = 0.8$ mm, $t_2 = 0.2$ mm, g = 0.4 mm, and refractive index of substrate $n = 3.4$. (b) Patch and wire elements with design parameters $D_1 = 5/3$ mm, $D_2 = 5$ mm, t = 0.5 mm, $t_1 = 0.8$ mm, $t_2 = 0.2$ mm, g = 0.4 mm, and refractive index of substrate $n = 3.4$. Design parameters of additional patch elements: A = 4.4 mm.

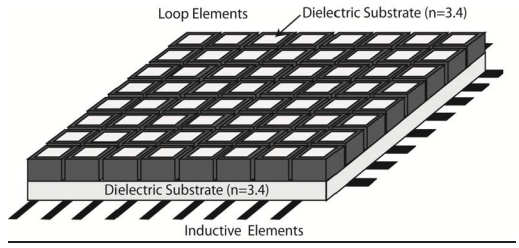

Fig. 15. Sensor platforms consisting of periodic arrays of loop and wire elements.

capacitance value of $C_s \ll C$, thereby negating the effects of ω_0 and B (Fig. 13(a)). However, if we increase the size of the additional patch elements to A = 4.4 mm, the transmission behavior affected by C_s is more evident because $C \sim C$ in Eqns. (15) and (16). Thus, the use of a sensing architecture with complementary loop elements provides a small resonant frequency $\omega_0 \sim 5.1$ GHz and narrowband spectrum $B \sim 0.277$, as shown in Fig. 13(b).

VIII. Design of Metamaterial Sensors Using Complementary Loop Elements and Loop Elements

In this section, we consider sensing architectures based on loop elements and complementary loop elements. As mentioned in the previous section, thicker capacitive elements ($t_1 = 0.8$ mm) can be used to generate a narrowband spectrum and a low resonant frequency. Fig. 14 shows design architectures with wire elements and complementary loop elements. In order to examine the transmission behavior modified by C_s, we use a periodic array of capacitive elements with a periodic distance $D_1 = 5/3$ mm within a unit cell to provide a large $\Delta\omega_0$. As expected, the complementary loop elements provide a narrower band spectrum compared with that produced by wire elements. However, the capacitance increase due to the use of the complementary loop elements provides a smaller $\Delta\omega_0$ when compared with obtained with wire elements.

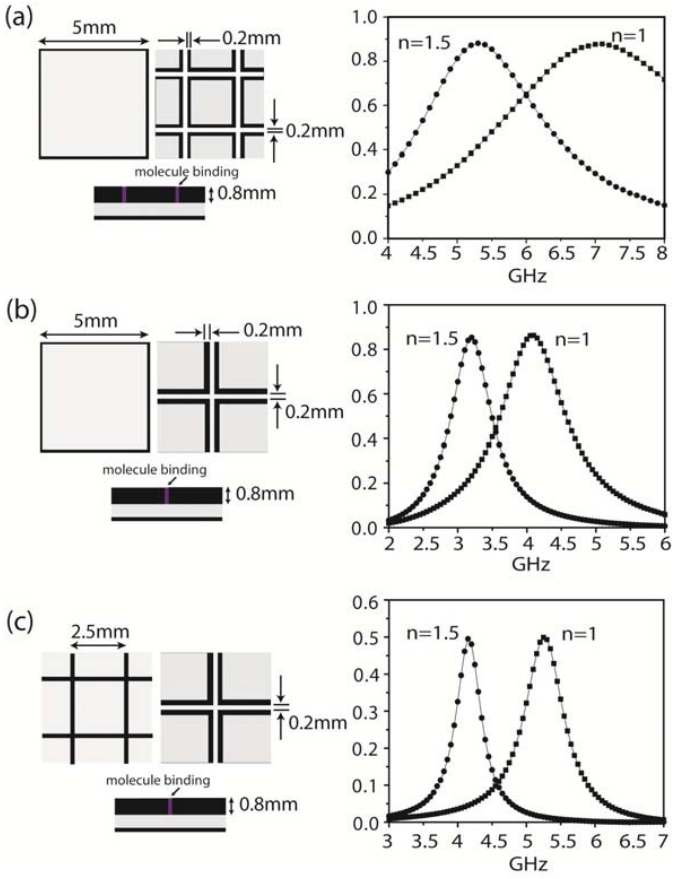

Fig. 16. Transmission ratios for three different sensing architectures obtained with normal incident frequency without (n = 1) and with molecule binding (n = 1.5). (a) Loop and wire elements with design parameters $D_1 = 2.5$ mm, $D_2 = 5$ mm, t = 0.5 mm, $t_1 = 0.8$ mm, $t_2 = 0.2$ mm, g = 0.2 mm, and refractive index of substrate $n = 3.4$. (b) Loop and wire elements with design parameters $D_1 = 5$ mm, $D_2 = 5$ mm, t = 0.5 mm, $t_1 = 0.8$ mm, $t_2 = 0.2$ mm, g = 0.2 mm, and refractive index of substrate $n = 3.4$. The width of loop elements is $w_2 = 0.2$ mm. (c) Loop and wire elements with design parameters $D_1 = 5$ mm, $D_2 = 2.5$ mm, t = 0.5 mm, $t_1 = 0.8$ mm, $t_2 = 0.2$ mm, g = 0.2 mm, and refractive index of substrate $n = 3.4$. The width of loop elements is $w_2 = 0.2$ mm.

TABLE II
PHYSICAL SENSING PARAMETERS FOR DEVICE ARCHITECTURES SHOWN IN FIG. 16

	Resonant Frequency (ω_0)	Unit Cell at ω_0	Resonant Frequency Shift ($\Delta\omega_0$)	Bandwidth ($\omega_H - \omega_L/\omega_0$)	Transmission Ratio (P_T/P_I)
Type I	7.1	0.116λ	1.9 GHz	Broadband 0.528	0.88
Type II	4.1	0.070λ	0.9 GHz	Narrowband 0.28	0.86
Type III	5.25	0.088λ	1.1 GHz	Narrowband 0.122	0.50

Finally, we investigate sensing architectures based on loop elements and wire elements, as shown in Fig. 15. For example, we insert a dielectric substrate ($n = 3.4$) within the loop elements. In principle, highly selective sensing architectures can be achieved by modulating the refractive index n at the subwavelength metallic gaps between the loop elements.

Fig. 16 shows the calculated transmission ratios of sensing architectures based on subwavelength loop elements. The basic sensing properties for the three types of loop elements are summarized in Table II. It is to be noted that each of the sensing architectures provides a unique performance advantage in terms of $\Delta\omega_0$, device size, and spectral response. For instance, Type I provides a large $\Delta\omega_o \sim 1.9$ GHz at $\delta n \sim 0.5$ with broadband spectrum $B \sim 0.528$ and transmission $T \sim 0.88$, However, type II corresponds to highly miniaturized elements with $D \sim 0.070\lambda$ with a small narrowband spectrum value of $B \sim 0.28$, a small value of $\Delta\omega_o \sim 0.9$ GHz at $\delta n \sim 0.5$ and transmission $T \sim 0.86$. Finally, in terms of enhanced selectivity, type III corresponds to a highly narrow spectral bandwidth $B \sim 0.122$ with $D \sim 0.088\lambda$ and a low transmission $T \sim 0.50$.

IX. CONCLUSION

In summary, the paper introduces a design methodology for simple wireless sensing platforms based on parallel-*LC* building blocks using periodic arrays of capacitive and inductive elements. Specifically, the paper discusses the design methods of various sensing architectures based on patch, wire, loop, and complementary loop elements instead of split-ring resonators (SRRs). With the use of these architectures, one can easily design a sensor of specified selectivity and sensitivity. Even though signal to noise ratio (SNR) is decreased by opaque materials with finite conductivities, these approaches can be applied to a new type of label-free sensing platforms for biomolecular and chemical-molecule sensing applications. Furthermore, the merit of these architectures is that it leads to the miniaturization of circuit elements at a subwavelength scale and provides a very narrowband and the proposed design methods can be applied to other frequency ranges such as the terahertz or infrared spectrum by appropriately scaling the dimensions of the periodic *LC* elements. Therefore, scalability of the proposed design to customize the applications in different frequency bands is a major advantage of the proposed design methodology.

REFERENCES

[1] D. R. Smith, J. B. Pendry, and M. C. K. Wiltshire, "Metamaterials and negative refractive index," *Science*, vol. 305, no. 5685, pp. 788–792, Aug. 2004.
[2] D. R. Smith, W. J. Padilla, D. C. Vier, S. C. Nemat-Nasser, and S. Schultz, "Composite medium with simultaneously negative permeability and permittivity," *Phys. Rev. Lett.*, vol. 84, no. 18, pp. 4184–4187, May 2000.
[3] J. B. Pendry, "Negative refraction makes a perfect lens," *Phys. Rev. Lett.*, vol. 85, pp. 3966–3969, Oct. 2000.
[4] N. Fang, H. Lee, C. Sun, and X. Zhang, "Sub-diffraction-limited optical imaging with a silver superlens," *Science*, vol. 308, no. 5721, pp. 534–537, Apr. 2005.
[5] S. P. Burgos, R. de Waele, A. Polman, and H. A. Atwater, "A single-layer wide-angle negative-index metamaterial at visible frequencies," *Nature Mater.*, vol. 9, pp. 407–412, May 2010.
[6] N. Fang, D. J. Xi, J. Y. Xu, M. Ambati, W. Srituravanich, C. Sun, and X. Zhang, "Ultrasonic metamaterials with negative modulus," *Nature Mater.*, vol. 5, pp. 452–456, Jun. 2006.
[7] D. Schurig, J. J. Mock, B. J. Justice, S. A. Cummer, J. B. Pendry, A. F. Starr, and D. R. Smith, "Metamaterial electromagnetic cloak at microwave frequencies," *Science*, vol. 314, no. 5801, pp. 977–980, Nov. 2006.

[8] J. B. Pendry, D. Schurig, and D. R. Smith, "Controlling electromagnetic fields," *Science*, vol. 312, no. 5781, pp. 1780–1782, Jun. 2006.
[9] H. Tao, E. A. Kadlec, A. C. Strikwerda, K. B. Fan, W. J. Padilla, R. D. Averitt, E. A. Shaner, and X. Zhang, "Microwave and Terahertz wave sensing with metamaterials," *Opt. Exp.*, vol. 19, no. 22, pp. 21620–21626, Oct. 2011.
[10] C. Debus and P. H. Bolivar, "Frequency selective surfaces for high sensitivity terahertz sensing," *Appl. Phys. Lett.*, vol. 91, no. 18, pp. 184102-1–184102-3, Oct. 2007.
[11] H. Tao, L. R. Chieffo, M. A. Brenckle, S. M. Siebert, M. K. Liu, A. C. Strikwerda, K. B. Fan, D. L. Kaplan, X. Zhang, R. D. Averitt, and F. C. Omenetto, "Metamaterials on paper as a sensing platform," *Adv. Mater.*, vol. 23, no. 28, pp. 3197–3201, Jul. 2011.
[12] K. Sarabandi and N. Behdad, "A frequency selective surface with miniaturized elements," *IEEE Trans. Antennas Propag.*, vol. 55, no. 5, pp. 1239–1245, May 2007.
[13] F. Bayatpur and K. Sarabandi, "Single-layer high-order miniaturized-element frequency-selective surfaces," *IEEE Trans. Microw. Theory Tech.*, vol. 56, no. 4, pp. 774–781, Apr. 2008.
[14] F. Bayatpur and K. Sarabandi, "Tuning performance of metamaterial-based frequency selective surfaces," *IEEE Trans. Antennas Propag.*, vol. 57, no. 2, pp. 590–592, Feb. 2009.
[15] F. Bayatpur and K. Sarabandi, "Multipole spatial filters using metamaterial-based miniaturized-element frequency-selective surfaces," *IEEE Trans. Microw. Theory Tech.*, vol. 56, no. 12, pp. 2742–2747, Dec. 2008.
[16] J. D. Baena, J. Bonache, F. Martin, R. M. Sillero, F. Falcone, T. Lopetegi, M. A. G. Laso, J. Garcia-Garcia, I. Gil, M. F. Portillo, and M. Sorolla, "Equivalent-circuit models for split-ring resonators and complementary split-ring resonators coupled to planar transmission lines," *IEEE Trans. Microw. Theory Tech.*, vol. 53, no. 4, pp. 1451–1461, Apr. 2005.
[17] D. Cai, Y. Shang, H. Yu, and J. Ren, "80 GHz on-chip metamaterial resonator by differential transmission line loaded with split ring resonator," *Electron. Lett.*, vol. 48, no. 18, pp. 1128–1130, Aug. 2012.
[18] W. Fei, H. Yu, Y. Shang, and K. S. Yeo, "A 2-D distributed power combining by metamaterial-based zero phase shifter for 60-GHz power amplifier in 65-nm CMOS," *IEEE Trans. Microw. Theory Tech.*, vol. 61, no. 1, pp. 505–516, Jan. 2013.
[19] I. Bardi, R. Remski, D. Perry, and Z. Cendes, "Plane wave scattering from frequency-selective surfaces by the finite-element method," *IEEE Trans. Magn.*, vol. 38, no. 2, pp. 641–644, Mar. 2002.

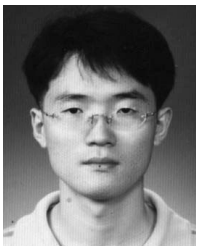

Kyungjun Song received the Ph.D. degree from the University of Michigan, Ann Arbor, MI, USA, in 2010. He is currently a Senior Researcher of Nature-Inspired Nano-convergence Mechanical System Division, Korea Institute of Machinery and Materials, Seoul, Korea. His current research interests include metamaterials, flexible devices, plasmonics, frequency selective surfaces, photonic crystals, and nature-inspired antireflection surfaces.

Pinaki Mazumder (F'99) received the Ph.D. degree in electrical and computer engineering from the University of Illinois at Urbana-Champaign, Urbana, IL, USA, in 1988, and the M.S. degree in computer science from the University of Alberta, Edmonton, AB, Canada, the B.S. degree in electrical engineering from the Indian Institute of Science, Bangalore, and the B.Sc. degree (Hons.) in physics from Guwahati University, Guwahati, India. Currently, he is a Professor of electrical engineering and computer science with the University of Michigan, Ann Arbor, MI, USA, where he has been teaching for the past 25 years. He was with the National Science Foundation serving as the Lead Program Director of Emerging Models and Technologies Program in the CISE Directorate as well as leading the Quantum, Molecular and High Performance Simulation Program in the Engineering Directorate. He was with Industrial R&D Laboratories which included AT&T Bell Laboratories, USA, and Bharat Electronics Ltd., India, for six years. He spent his sabbatical at Stanford University, Stanford, CA, USA. University of California at Berkeley, Berkeley, CA, USA, and NTT Center Research Laboratory, Japan. He has published over 260 technical papers and four books on various aspects of VLSI technology and systems. His current research interests include CMOS VLSI design, semiconductor memory systems, CAD tools and circuit designs for emerging technologies, including quantum MOS, spintronics, plasmonics, and resonant tunneling devices.

His inventions in testable DRAM circuits, in-line accelerated testing procedures for high-density RAM chips, and testing of embedded ROM and SRAM through JEDEC boundary scan ports are widely used by memory and FPGA manufacturers. His research in biology-inspired VLSI layout synthesis, self-healing VLSI design and self-repairable memory compilers has made commercial impact. In revolutionary emerging technologies, he has made sustained impact for the past 20 years by collaborating with multiple leading researchers in universities and companies. His research group has developed a Quantum SPICE simulator to design several innovative quantum tunneling based circuits that were fabricated from many U.S. companies. He was a recipient of Digital's Incentives for Excellence Award, the BF Goodrich National Collegiate Invention Award, and the DARPA Research Excellence Award. He is an AAAS Fellow (2007) for his distinguished contributions to the field of VLSI.